

Effects of the Substitutions and Vacany Defects on the Stable monolayer structures of Black and Blue Arsenic Phosphorus: A First Principles Study

Zhaleh Benam,^{1,*} Handan Arkin,^{1,†} and Ethem Aktürk^{2,3,‡}

¹*Department of Physics Engineering, Faculty of Engineering,
Ankara University, Tandoğan, 06100 Ankara, Turkey*

²*Department of Physics, Adnan Menderes University, 09100 Aydın, Turkey*

³*Nanotechnology Application and Research Center,
Adnan Menderes University, 09100 Aydın, Turkey*

We investigate two dimensional monolayer structures of arsenic phosphorus (AsP) by means of first principles plane wave method within density functional theory using the generalized gradient approximation. Two structures of arsenic phosphorus are taken into account which are called buckled (B-AsP) and puckered (Pu-AsP). From our numerical calculations we predicted the optimized states of a single-layer buckled and puckered honeycomb like allotropes of AsP. We demonstrate that buckled and puckered arsenic phosphorus are semiconducting single layers with band gap energies 1.858 eV and 0.924 eV, respectively. Especially, we have found that the puckered monolayer has a direct band gap. Furthermore, we examined the electronic and magnetic properties of various kind of point defects including single and double vacancies, antisite and substitutions on both buckled and puckered arsenic phosphorus. We conclude that AsP monolayers can attain magnetic state with vacancies and the semiconductor nature can turn into metal with diverse defect types. In considered system also the band gap of B-AsP can be tuned from metal character to 1.858 eV and for Pu-AsP from metal to 0.924 eV which these ranges are especially important for radar and atmospheric applications.

I. INTRODUCTION

The two dimensional monolayer honeycomb structures have exceptional properties and thus attracted a growing interest with their promising applications in nanotechnology. Recent studies in nanoscale physics have aimed the discovering new monolayer materials and revealing their properties under different conditions. Among these materials, graphene, which is a single layer honeycomb structure of carbon, has attracted great interest in various fields ranging from electronics to biotechnology due to its unique properties, such as high mechanical strength, chemical stability, and exceptional ballistic conductance [1, 2]. The search for the contender of graphene has led to the prediction/synthesis of new single-layer, crystalline nanostructures, which do not exist in nature. Silicene, germanene, stanene, namely graphene analogs of group IV or V elements [3–7]; h-BN analogs of group IV-IV, III-V, and II-VI compounds [8]; graphyne [9–11] and the auxetic piezoelectric 2D material silicatene with negative Poisson's ratio [12, 13] have been actively studied. Additionally, transition-metal dichalcogenides have proven to be superior than graphene in specific optoelectronic applications [14–17]. Especially, the silicene and germanene [4] have attained significant interest due to their nonmagnetic semimetallic behavior with linearly crossing π and π^* bands at Fermi level which is similar to graphene and due to their compatibility with silicon-based micro-electronic industry. In addition, two dimensional silicon carbide (SiC) and germanium carbide (GeC) honeycomb structures have been reported theoretically as stable [8, 18–20]. However, the electronic structure of graphene, and silicene, germanene as well have zero band gap, which restrain the ability and applications of them.

More recently, the fabrication of field effect transistors using micrometer-sized flakes consisting of two and three layers of black phosphorus [21] and their theoretical analysis [22, 23] revealing the stability of its single-layer allotropes brought group V elements into the focus. In contrast to the zero band gap of honeycomb lattices of group-IV elements, monolayer honeycomb structures of group-V elements such as Phosphorene [24], Arsenene [25] and Antimonene [26] are direct and indirect band gap semiconductors, respectively and they were found as stable [24–26] and the mechanical and electronic [27] properties were investigated. Because of direct or indirect band gap properties, these honeycomb monolayer structures can be promising materials for digital circuits and light-emitting diodes.

To date, these 2D layered materials have covered a wide electromagnetic spectral range including metals, semimetals,

*E-mail: zhaleh.benam@gmail.com

†E-mail: holgar@eng.ankara.edu.tr

‡E-mail: ethem.akturk@adu.edu.tr

semiconductors, and insulators. Specifically, monolayer graphene is a semimetal which exhibits a zero band gap in its natural states and strong electrical field can be used in order to create a band gap in bilayer graphene [28]. Few-layer and/or monolayer structures of group V elements, including phosphorene and arsenene, are emerging as promising candidates for two-dimensional (2D) electronic materials application [29–33]. Different from semimetallic graphene, these systems display a nonzero band gap while still maintaining a relatively high carrier mobility [34–37]. One of the newest members of the 2D layered material family is black phosphorus, which is a semiconductor exhibiting a moderate band gap of around 0.3 eV in its bulk form and up to 2.2 eV as in a monolayer [38], further pushing the band gap of single layered materials to the middle-wavelength infrared regime. Therefore, a broad spectral range has now been covered by the above mentioned layered materials. Although a wide range in electromagnetic spectrum has been covered by these 2D monolayer materials, there is still a big need to different smart materials because of the light radars and atmospheric applications in the longwavelength spectrum range. On the other hand, because of its direct band gap, black phosphorus is currently considered the best material on-chip detectors. Besides all of these advantages, few-layer black phosphorus samples demonstrate high reactivity, resulting in a fast degradation of crystals under ambient conditions and while being chemically much less reactive, layered gray arsenic also display a significant band gap. In order that reason, the combination of black phosphorus and gray arsenic may exhibit phase coexistence that should bring an unexpected richness in both structural and electronic properties, in comparison to pristine of phosphorene and arsenene, has already been shown by the end of year 2015 [39]. This structure has been called black arsenic phosphorus and the honeycomb structure which can also be exist in nature is called blue arsenic phosphorus.

Although both buckled and puckered arsenene monolayers are stable structures which are shown by phonon spectrums and with their cohesive energies, they possess indirect band gaps of 0.831 eV and 1.635 eV, respectively [25]. In this paper, motivating by recent studies of phosphorene and arsenene, our aim is modifying the indirect gap of arsenene by making black arsenic phosphorus or in other words by substitution of arsenic atoms to phosphorene. Additionally, we are thinking that the electronic properties of these new phases of arsenic phosphorus can be tuned further and can be functionalized by substitution and vacancy processes. Because previous experimental and theoretical studies have proven that bare 2D monolayer structures can be functionalized through point defects to attain crucial physical and chemical properties for diverse applications.

On this object, we present *ab initio* calculations of the arsenic phosphorus allotropes in the frame of first principles calculations. Beside Si, Ge, Sn monolayers and with the development of experimental technology, AsP monolayer have the advantage of manufacturing by exfoliating crystalline black phosphorus which has been shown recently by Liu et. al. [40]. In this study, a new synthetic route was used for the synthesis of AsP layers which uses gray arsenic and red phosphorus as starting materials. Therefore AsP is chosen as the research objective of interest here. We investigate the stability and electronic properties of the 2D honeycomb structures. We have found that two honeycomb structures called buckled (B-AsP) and puckered (Pu-AsP) arsenic phosphorus are stable and the puckered AsP structure has a direct band gap. Furthermore we focus on investigating the effects of the point defects in the physical properties of black and blue arsenic phosphorus monolayers by first principles calculations. In all structures the geometric optimization are done and the reconstruction, the effects on the electronic properties have been discussed. In summary, the works discussed in this letter may open a new page in the field of material science by predicting new smart surfaces.

The rest of the paper is organized as follows. In Section II the calculation methods are described in detail. Then, Section III contains the results and discussion. Finally, Section IV concludes the paper with a summary of our findings.

II. CALCULATION METHODS

The structural stability and the electronic properties of the Arsenic Phosphorus monolayer structures have been investigated by means of first-principles plane-wave calculations within density functional theory (DFT) using projector augmented wave (PAW) potentials [41]. The exchange-correlation potential is approximated by generalized gradient approximation (GGA) using Perdew-Burke-Ernzerhof (PBE) parametrization [42]. All numerical results have been obtained by using Quantum Espresso software [43]. A plane-wave basis set with the kinetic energy cutoff $\hbar^2(\mathbf{k}+\mathbf{G})^2/2m = 65$ Ry is used. Pseudopotentials with $4s^23d^{10}4p^3$ and $3s^23p^3$ valence electron configurations for As and P atoms were used, respectively. All structures are treated using periodic boundary conditions.

The Brillouin zone has been sampled by $(21 \times 21 \times 1)$ and $(7 \times 7 \times 1)$ special mesh points in \mathbf{k} -space by using Monkhorst-Pack scheme [44] for (1×1) and (4×4) AsP cells, respectively. All atomic positions and lattice constants are optimized by using BFGS quasi-Newton algorithm [45] where the total energy and forces are minimized. The convergence criteria for energy is chosen as 10^{-8} Ry between two consecutive steps. The maximum Hellmann-Feynman forces acting on each atom is less than 0.001 Ry/au upon ionic relaxation. The maximum pressure on the unit cell is less than 0.5 kbar. Gaussian type Fermi-level smearing method is used with a smearing width of 0.1 eV.

III. RESULTS AND DISCUSSION

A. Structural properties of the monolayers

Graphene is a planar honeycomb structure since it form pure sp^2 hybridization. On the other hand except graphene the other elemental honeycomb monolayers form buckled structures for example the silicene and germanene are the most popular ones. In addition, which has recently predicted, the phosphorene made of black phosphorus has a puckered structure and its buckled structure namely blue phosphorus has been investigated by first principles study [24]. From this purpose, we take two structures of arsenic phosphorus into account and show the optimized geometric structures for the cases a) buckled b) puckered in Fig.1 from side view and from top view. The structural parameters corresponding to the two different structures which are under consideration in this study are given in Table I. The lattice constants of optimized orthorhombic structure for Pu-AsP in equilibrium are $a = 3.50$ and $b = 4.68$ Å which are about 4 percent longer than the lattice vectors of black phosphorene and shorter than the lattice vectors of black arsenene. For the hexagonal structure B-AsP in equilibrium are $a = b = 3.46$ Å. The B-AsP is again 4 percent longer than the blue phosphorene and shorter than blue arsenene. The bond distance between As and P atoms are $d_{1As-P} = 2.374$ Å and $d_{2As-P} = 2.382$ Å for Pu-AsP, $d_{As-P} = d = 2.393$ Å for B-AsP. We found that the bond lengths of both puckered and buckled monolayers are smaller than its counterpart of arsenenes and slightly bigger than black- and blue-phosphorene.

To prove the stability of the monolayers, we calculated their cohesive energies defined as $E_{coh} = (nE_{As} + nE_P - nE_{AsP})/2n$, where E_{As} , E_P and E_{AsP} are the total energies of single As atom, a single P atom, and a As-P pair in the AsP monolayer, respectively. The puckered and buckled monolayer structures have a cohesive energies 4,782 eV and 4,802 eV respectively per As-P pair and these values are very similar for the different monolayer structures which are stable and manufactured successfully. These values are clear evidence that AsP monolayers are strongly bonded networks. To check the structure optimizations, we increase the degrees of freedoms to 4x4 cells which we got the same geometry and cohesive energy.

In mean, we investigate here a previously unknown structure of arsenic phosphorus which called buckled structure. This structure is a honeycomb structure like graphene and it is as stable as puckered structure. Whereas these structures is hexagonal structures closely related to graphene, the main advantage of these structures are those band gaps which are approximately in the range of 1.0 - 2.0 eV. Although the band gaps are typically underestimated with the DFT calculations from the literature the general trend is confirmed, and the black- and blue arsenic phosphorus have larger band gaps than the 2D counterparts where additionally the puckered structure has the advantage of direct band gap. Because the band gaps of most explored 2D materials exhibite moderate band gaps around 0.3 eV, which greatly restricts applications based on semiconductor and optoelectronic device technology.

B. Electronic structure

Here we carried out the electronic band structure and in order to understand the contributions of atomic orbitals to the elctronic states we have plotted the corresponding total (DOS) and partial (PDOS) density of states for the buckled and puckered monolayers as shown in Fig.2a, Fig.2b, respectively. From the electronic band structures it is obviously seen that puckered AsP is direct band gap semiconductor with a band gap of 0.924 eV whereas buckled AsP is indirect band gap semiconductor with a band gap of 1.858 eV. It is observed from the PDOS plots that the electronic states both in puckered and buckled structures have contributions from s and p orbitals near the Fermi energy, but the s orbital contribution is very small compared to p orbital contribution. This is very well known feature of monolayer honeycomb systems such as germanene, silicene and phosphorene, where the sp^2 -like bonds form a nonplanar honeycomb structures different than graphene. An indirect band gap in buckled AsP resembles that of buckled (blue) phosphorene and arsenene. The valence band maximum lies at the Γ -point, and the conduction band minimum lies along $\Gamma - M$ direction. Same situation are also seen both in buckled phosphorene and arsenene. Only the band gap is higher than arsenene in our case. But we could not exactly compare our value with the indirect band gap of buckled phosphorene, because its band gap was given as approximate value [24]. On the other hand, the direct gap semiconducting behaviour of puckered AsP is distnctly different from the indirect band gap behaviour of puckered arsenene. Its looks like mostly to puckered phosphorene. Because both structures have direct band gaps at the Γ -point with band gaps of 0.91 eV for puckered phosphorene and 0.92 eV for puckered AsP, respectively. But, additionally we note that, puckered AsP structure have two seperate valence band and conduction band edges near the Fermi level. The maximum of the valence band and the minimum of the conduction band occur along $\Gamma - Y$ direction and at the Γ -point which both are direct edges. This fact is distnctly different also from the electronic band structure of phosphorene which have only direct edge at the Γ -point.

C. Investigation of the Defects structures

To investigate the effects of the defects we optimized 4x4 supercells of the buckled and puckered AsP monolayers. Such size for the supercells provide sufficient distance for the examination of the defects. As presented in Fig.1 the lattice constant and the bond length of the 4x4 supercell buckled AsP which contains 16 As and 16 P atoms, are found to be $a = b = 13.84$ Å and $d_{As-P} = 2.393$ Å respectively. The cohesive energy is found to be the same with the unit cell. The puckered AsP 4x4 super cell contains 32 As atoms and 32 P atoms. The lattice constants for this structure are $a = 14.00$ Å and $b = 18.72$ Å and the bond length is $d_{As-P} = 2.382$ Å same with the unit cell. As illustrated in Fig.2 valance band maximum and conduction band minimum consist main contribution of p orbitals of As and P atoms near Fermi level. Single atom vacancies and antisite defects are dominate defects during the fabrication of single layer materials, or some experiment can cause these defects. The presence of these defects can change electronic and magnetic properties of the materials. We examine in this section that introducing various defects into buckled and puckered AsP monolayer can cause to crucial changes in the electronic and magnetic properties. Firstly, all defect structures are subjected to geometrical optimization and we calculated their cohesive energies which the expression is given before and formation energy for the substitution defect X_Y , where the atom Y occupies the site of atom X, by using the equation below,

$$E_{form} = E_{substrate+X_Y} - E_{substrate} + E_Y - E_X.$$

Here, the energy for the single As and P atoms are calculated from the As-rich structure and from the P-rich structure, respectively. We take arsenene monolayer as As-rich structure and phosphorene monolayer for the P-rich structure. The considered various defects and the label of them are given as follows:

- Vacancy: An atom As (P) subtract from its position in the monolayer network labelled as $V_{As}(V_P)$.
- Substitution: When As(P) atom placed instead of P(As) atom labelled as $As_P(P_{As})$.
- Antisite: When the position of neighboring As and P atoms are exchanged ($As \leftrightarrow P$).

D. Defect Structures on B-AsP monolayer

Firstly, we examine the As vacancy defect structure, which the fully relaxed structure is presented in Fig.3a. After optimization, three P atoms around the vacancy are approaching to each other, so the P-P distance changed to 3.237 Å and to 3.192 Å which in the pristine state was 3.460 Å. We found the bond length of As-P distance as approximately 2.361 Å which differs from the pristine monolayer while in pristine monolayer the As-P distance was 2.393 Å. The accurate structural distances are shown in figures in detail. As shown in TableII, since the cohesive energies of vacancies are almost equal, formation energy of V_{As} is the highest among the others. To determine the electronic properties of the system we obtained the density of states (DOS) as presented in Fig.3a. As vacancy induces a very small local magnetization ($0.04 \mu_B$) and the system turns to metallic character. This is the only defect state among the others on B-AsP monolayer which turns into magnetic state. As seen in Fig.3 in detail on can concluded that two defect states appear in the band gap. While one occurs from contributions of $p_x - p_y$ and p_z orbitals of P atoms around the vacancy, the other state at the higher energy level are mixed state of s , $p_x - p_y$ and p_z orbitals of P atoms around vacancy. According to Löwdin charge analysis [46], the excess charge on P atoms around vacancy, which is calculated by subtracting the charge at the atom from its valance charge, is 0.03 electrons while the other P atoms have 0.01 electrons excess charge in the bare state.

The second defect structure under consideration is P vacancy (V_P) which three dangling bonds occur with As-As = 3.328 Å distance, as seen in Fig.3b. All the other bond lengths are shown in figure. This defect state is nonmagnetic and shows also metallic character. Like the V_{As} case, two defect states occur at the band gap, while first consist of p_x, p_y, p_z orbitals of As atoms around the vacancy and the other has also contribution from the s orbitals of the As atoms around vacancy. According to Löwdin charge population analysis, As atoms around vacancy gives 0.06 electrons to the surrounding substrate. Additionally the most energetically favourable vacancy defect state is the V_P state.

Energetically second favourable vacancy defect state among the considered states is the divacancy V_{AsP} , which is the state of lacking both As and P atoms in the network. After the geometric optimization the hexagonal structure is changed to an octagon and two pentagons, which is illustrated in Fig.3c with detailed bond length informations. This is also the case where we have the biggest lattice correction with respect to the bare monolayer. The V_{AsP} system has 0.847 eV band gap due to the defect states. As shown in Fig.3c these defects levels at around -0.75 eV and +0.70 eV have significant contributions from As_p and P_p orbitals. Löwdin analysis indicates that 0.10 electrons are transferred from As atoms and 0.001 electrons are transferred to P atoms around the vacancy.

The other kind of system has antisite defect, which we exchange the positions of the neighbouring As and P atoms ($As \leftrightarrow P$) in the network is presented in Fig.4a. We have detected that negligible bond length elongation occur in that system. Also there is no lattice correction. The d_{As-P} bond length changes only from 2.393 Å to 2.394 Å. The P-P bond distance and As-As bond distance are 2.261 Å and 2.506 Å respectively. Therefore the band gap is also affected minimal only slightly from 1.858 eV to 1.831 eV. As the other cases the orbital contributions of As and P atoms around defects are shown in Fig.4a. The excess charges on the exchanged atoms are 0.11 and 0.02 electrons, respectively. These results with its small formation energy implies that this structure can be occur or dominate defect during the fabrication of AsP monolayer.

The other kind of defect is obtained by substitution of As atom instead of P atom in the monolayer (As_P). In the fully optimized structure of As_P (Fig.4b, four As atoms are reorganized and they bonds to each other with a bond length of As-As = 2.495 Å. The As-P bond length is nearly the same with the pristine system (2.395 Å and 2.384 Å which are denoted in the figure). There is no lattice correction. Also this defect cannot induce any magnetization and the band gap changes very slightly only to 1.804 eV. While the As atom at the central gives 0.08 electrons to the surrounding the others give 0.12 electrons.

Last considered defect for B-AsP monolayer is P_{As} , the As atom is replaced by P atom in the network, is shown in Fig.4c with its optimized structure. This structure has also similar geometry with the previous defect, where the bond length of As-P is again 2.384 Å and the P-P distance is approximately 2.268 Å. Also P_{As} structure is nonmagnetic and is semiconductor with a band gap 1.842 eV. In Fig.4c, we illustrate the electronic DOS of P_{As} which overlaps with As_P defect structure. According to the Löwdin analysis, the central P atom has 0.16 electrons, while the other P atoms has -0.01 electrons excess charges.

E. Defect Structures on Pu-AsP monolayer

As in the B-AsP monolayer case, the first considered vacancy defect on Pu-AsP monolayer is As vacancy (V_{As}), illustrated in Fig.5a. In this defect structure the lattice constants a and b are changed from 14.00 Å to 13.95 Å and from 18.72 Å to 18.65 Å, respectively. The bond length of As-P atoms increases from 2.395 Å to 2.580 Å. Other structural distances are shown in figure. With these structural parameters this state is one of the most defected state among the others which one can also concluded from the formation energy. To discuss the electronic properties we obtained the density of states as presented in Fig.5a. This system is nonmagnetic. The defect states occurs at the Fermi level and has contributions from both P and As atoms around the vacancy. According to the Löwdin charge population analysis, the excess charge on the P atoms around the vacancy is -0.03 electrons.

In the V_P structure, we detect also lattice correction where the lattice constant are $a = 13.97$ Å and $b = 18.68$ Å. The accurate lengths related with the structure are given in the figure. This state is magnetic with a magnetization of $1.19 \mu_B$. The band gap significantly decreases from 0.924 eV to zero eV in spin-up channel while a defect state from the spin-down channel is about +0.25 eV from contributions of the p_y orbital of As atoms around the vacancy. The As atoms around the vacancy gives 0.08 to the surrounding network where the other As atoms give 0.16 electrons.

The most energetically favourable state among the vacancies are the V_{AsP} structure with a formation energy value of 0.926 eV (Table II). After relaxation, we have found the new lattice parameters as $a = 13.94$ Å and $b = 18.64$ Å, respectively. The As-P bond distance is approximately 2.37 Å, where the newly constructed P-P and As-As bond distances are 2.298 Å and 2.676 Å. In distinction to the other vacancy defects structures, divacancy structure is nonmagnetic, with a larger band gap of 1.086 eV with respect to the bare Pu-AsP monolayer as well as with respect to the other defected structures of Pu-AsP. The defect states above and below the Fermi level has main contributions from As_p and P_p orbitals around the vacancy. Each P (As) atom of P-P (As-As) bond has excess charge of -0.03 (0.11) electrons.

The other kind of defect considered distinctively from the vacancies is the antisite defect where the P and As atoms are exchanged (Fig.6a). We employ two different exchanging to the neighbouring P and As atoms. In the first type the exchanging is done on the x-direction and in the second one the exchanging is done on the y-direction. We detect no difference between these two defect structures at the end of the relaxation. On both system there are neither lattice constant correction nor bond distance change between the P and As atoms. These defect structures are as stable as the bare Pu-AsP monolayer structure is. The defect structures are nonmagnetic and have 0.91 eV band gaps. The exchanged atoms both give 0.06 electrons to the surrounding substrate. The formation energies are very small, so that there are no significant change due to these defect type.

Next considered defect structures are As_P and P_{As} (As (P) atom is placed instead of P (As) atom site) where both have minimal lattice corrections (Table III) have shown in Fig.6b and c with those related bond lengths. These structures are nonmagnetic and have 0.912 eV and 0.921 eV band gaps, respectively. According to the Löwdin charge analysis, in As_P (P_{As}) system the As (P) atom has excess charge of 0.03 (0.09) electrons. These defect structures have very similar properties unlike their formation energies. From the formation energies As_P defect is more dominate

defect in comparison to P_{As} defect.

IV. CONCLUSIONS

In conclusion, based on the first principles plane wave calculation within the density functional theory, black and blue arsenic phosphorus monolayer structures are predicted. We show the structural and electronic properties of these monolayer structures. The black AsP monolayer is found to be a direct semiconductor with a band gap of 0.924 eV while the blue counterpart has a indirect band gap of 1.804 eV. Additionally we investigated the electronic and magnetic properties of various kind of point defects including single and double vacancies, antisite and substitutions on both puckered and buckled arsenic phosphorus. Our first principles density functional theory calculations show that the electronic and magnetic properties of pristine B-AsP and Pu-AsP monolayers can be adjustable by single and double vacancies, antisite and substitution defects. The nonmagnetic semiconductor nature of both monolayers can be transformed into metallic or narrow gap semiconductor upon defected structures. The band gaps can be tuned from metal character to 1.858 eV for B-AsP and from metal to 0.924 eV for Pu-AsP which these ranges are especially important for radar and atmospheric applications. Furthermore, the vacancy defects induces magnetic moments in both monolayers.

V. ACKNOWLEDGEMENT

Computing resources used in this work were provided by the TUBITAK (The Scientific and Technical Research Council of Turkey) ULAKBIM, High Performance and Grid Computing Center (Tr-Grid e Infrastructure).

-
- [1] Geim, A. K.; Novoselov, K. S. The Rise of Graphene. *Nat. Mater.* 2007, 6, 183-191.
 - [2] Novoselov, K. S.; Geim, A. K.; Morozov, S. V.; Jiang, D.; Zhang, Y.; Dubonos, S. V.; Grigorieva, I. V.; Firsov, A. A. *Science* 2004, 306, 666-669.
 - [3] E. Durgun, S. Tongay, and S. Ciraci, *Phys. Rev. B* 72, 075420 (2005).
 - [4] S. Cahangirov, M. Topsakal, E. Akturk, H. Sahin, and S. Ciraci, *Phys. Rev. Lett.* 102, 236804 (2009).
 - [5] P. Vogt, P. Depadova, C. Quaresima, J. Avila, E. Frantzeskakis, M. C. Asensio, A. Resta, B. Ealet, and G. Lelay, *Phys. Rev. Lett.* 108, 155501 (2012).
 - [6] V. O. Ozelik, E. Durgun, and S. Ciraci, *J. Phys. Chem. Lett.* 5, 2694 (2014).
 - [7] Y. Xu, B. Yan, H. J. Zhang, J. Wang, G. Xu, P. Tang, W. Duan, and S. C. Zhang, *Phys. Rev. Lett.* 111, 136804 (2013).
 - [8] H. Sahin, S. Cahangirov, M. Topsakal, E. Bekaroglu, E. Akturk, R. T. Senger, and S. Ciraci, *Phys. Rev. B* 80, 155-453 (2009).
 - [9] S. Tongay, S. Dag, E. Durgun, R. T. Senger, and S. Ciraci, *J. Phys.: Condens. Matter* 17, 3823 (2005).
 - [10] D. Malko, C. Neiss, F. Vines, and A. Grling, *Phys. Rev. Lett.* 108, 086804 (2012).
 - [11] V. O. Ozelik and S. Ciraci, *J. Phys. Chem. C* 117, 2175 (2013).
 - [12] V. O. Ozelik, S. Cahangirov, and S. Ciraci, *Phys. Rev. Lett.* 112, 246803 (2014).
 - [13] X. Xu, J. Zhuang, Y. Du, H. Feng, N. Zhang, C. Liu, T. Lei, J. Wang, M. Spencer, T. Morishita, X. Wang, and S. X. Dou, *Sci. Rep.* 4, 7543 (2014).
 - [14] P. Joensen, R. F. Frindt, and S. R. Morrison, *Mater. Res. Bull.* 21, 457 (1968).
 - [15] J. N. Coleman, M. Lotya, A. O. Neil, S. D. Bergin, P. J. King, U. Khan, and K. Young, *Science* 331, 568 (2011).
 - [16] C. Ataca and S. Ciraci, *J. Phys. Chem. C* 115, 13303 (2011).
 - [17] C. Ataca, H. Sahin, and S. Ciraci, *J. Phys. Chem. C* 116, 8983 (2012).
 - [18] E. Bekaroglu, M. Topsakal, S. Cahangirov, S. Ciraci, *Phys. Rev. B* 81 (2010) 075433.
 - [19] L. Sun, Y. Li, Z. Li, Q. Li, Z. Zhou, Z. Chen, J. Yang, J.G. Hou, *J. Chem. Phys.* 129 (2008) 174114.
 - [20] B. Xu, J. Yin, Y.D. Xia, X.G. Wan, Z.G. Liu, *Appl. Phys. Lett.* 96 (2010) 143111.
 - [21] L. Li, Y. Yu, G. J. Ye, Q. Ge, X. Ou, H. Wu, D. Feng, X. H. Chen, and Y. Zhang, *Nat. Nanotechnol.* 9, 372-377 (2014).
 - [22] Z. Zhu and D. Tomanek, *Phys. Rev. Lett.* 112, 176802 (2014).
 - [23] T. Low, A. S. Rodin, A. Carvalho, Y. Jiang, H. Wang, F. Xia, and A. H. Castro Neto, *Phys. Rev. B* 90, 075434 (2014).
 - [24] Z. Zhu and D. Tomanek, *Phys. Rev. Lett.* 112 (2014) 176802.
 - [25] C. Kamal and M. Ezawa, *Phys. Rev. B* 91 (2015) 085423.
 - [26] O. Üzengi Akturk, V. Ongun Özçelik, S. Ciraci, *Phys. Rev. B* 91 (2015) 234446.
 - [27] S. Zhang, Z. Yan, Y. Li, Z. Chen, H. Zeng, *Angew. Chem. Int. Ed.* 54 (2015) 3112, 3115.
 - [28] Y. Zhang , T. T. Tang , C. Girit , Z. Hao , M. C. Martin , A. Zettl , M. F. Crommie , Y. R. Shen , F. Wang , *Nature* 2009 , 459 , 820 .
 - [29] Narita, S.; Akahama, Y.; Tsukiyama, Y.; Muro, K.; Mori, S.; Endo, S.; Taniguchi, M.; Seki, M.; Suga, S.; Mikuni, A.; Kanzaki, H. *Physica B+C* 1983, 117-118, 422-424.
 - [30] Maruyama, Y.; Suzuki, S.; Kobayashi, K.; Tanuma, S. *Physica B+C* 1981, 105, 99-102.
 - [31] Liu, H.; Neal, A. T.; Zhu, Z.; Luo, Z.; Xu, X.; Tomanek, D.; Ye, P. D. *ACS Nano* 2014, 8, 4033-4041.
 - [32] Zhu, Z.; Guan, J.; Tomanek, D. *Phys. Rev. B: Condens. Matter Mater. Phys.* 2015, 91, 161404.
 - [33] Liu, B.; Kpf, M.; Abbas, A. N.; Wang, X.; Guo, Q.; Jia, Y.; Xia, F.; Weihrich, R.; Bachhuber, F.; Pielnhöfer, F.; Wang, H.; Dhall, R.; Cronin, S.; Ge, M.; Fang, X.; Nilges, T.; Zhou, C. *Adv. Mater.* 2015, 27, 4423-4429.
 - [34] Zhang, Y.; Tan, Y. W.; Stormer, H. L.; Kim, P. *Nature* 2005, 438, 201-204.
 - [35] S. P. Koenig, R. A. Doganov, H. Schmidt, A. H. Castro Neto and B. zylmaz, *Appl. Phys. Lett.*, 2014, 104, 103106.
 - [36] A.Castellanos-Gomez, L. Vicarelli, E. Prada, J. O. Island, K. L. Narasimha-Acharya, S. I. Blanter, D. J. Groenendijk, M. Buscema, G. A. Steele, J. V. Alvarez, H. W. Zandbergen, J. J. Palacios and H. S. J. van der Zant, *2D Mater.*, 2014, 1, 025001.
 - [37] F. Xia, H. Wang and Y. Jia, *Nat. Commun.* 2014, 5, 4458.
 - [38] X. M. Wang , A. M. Jones , K. L. Seyler , V. Tran , Y. C. Jia , H. Zhao , H. Wang , L. Yang , X. D. Xu , F. N. Xia , *Nat. Nanotechnol.* 2015 , DOI:10.1038/nnano.2015.71.
 - [39] Z. Zhu, J. Guan and D. Tomanek, *Nano Lett.*, 2015, 15, 6042.
 - [40] B. Liu, M. Köpf, A. Abbas, X. Wang, Q. Guo, Y. Jia, F. Xia, R. Weihrich, F. Bachhuber, F. Pielnhöfer, H. Wang, R. Dhall, S. Cronin, M. Ge, X. Fang, T. Nilges, C. Zhou, *Adv. Mater.* 27 (2015) 4423-4429.
 - [41] P.E. Blöchl, *Phys. Rev. B* 50 (1994) 17953.
 - [42] J.P. Perdew, K. Burke, M. Ernzerhof, *Phys. Rev. Lett.* 77 (1996) 3865.
 - [43] P. Giannozzi, S. Baroni, N. Bonini, M. Calandra, R. Car, C. Cavazzoni, D. Ceresoli, G.L. Chiarotti, M. Cococcioni, I. Dabo, A. Dal Corso, S. Fabris, G. Fratesi, S. de Gironcoli, R. Gebauer, U. Gerstmann, C. Gougoussis, A. Kokalj, M. Lazzeri, L. Martin-Samos, N. Marzari, F. Mauri, R. Mazzarello, S. Paolini, A. Pasquarello, L. Paulatto, C. Sbraccia, S. Scandolo, G. Sclauzero, A.P. Seitsonen, A. Smogunov, P. Umari, R.M. Wentzcovitch, *QUANTUM ESPRESSO: A Modular and Open-Source Software Project for Quantum Simulations of Materials*, *J. Phys: Condens. Matter* 21 (2009) 395502.
 - [44] H.J. Monkhorst, J.D. Pack, *Phys. Rev. B* 13 (1976) 5188.
 - [45] C.G. Broyden, The Convergence of a Class of Double-rank Minimization Algorithms 1. General Considerations, *Journal of Institute of Mathematics and Its Applications* 6 (1970) 76-90.

- [46] P.-O. Löwdin, J. Chem. Phys. 18 (1950) 365.
- [47] K. Momma, F. Izumi, VESTA 3 for three-dimensional visualization of crystal, volumetric and morphology data, J. Appl. Crystallogr. 44 (2011) 12721276.

Table 1: Calculated parameters for the two structures corresponding to Pu-AsP and B-AsP respectively. a , the lattice constant; $d(As - P)$, As-P distance; E , total energy; E_g , band gap.

Table 2: Calculated results for optimized defective structures of B-AsP monolayer; E_{coh} , cohesive energy; E_{form} , formation energy, a , corrected lattice constant; μ , magnetic moment per supercell in units of Bohr magneton (μ_B) (NM is for nonmagnetic systems).

Table 3: Calculated results for optimized defective structures of Pu-AsP monolayer; E_{coh} , cohesive energy; E_{form} , formation energy, a and b , corrected lattice constants; μ , magnetic moment per supercell in units of Bohr magneton (μ_B) (NM is for nonmagnetic systems).

Fig.1: Side view and top view of the structures of a) buckled B-AsP and b) puckered Pu-AsP.

Fig.2: Electronic band structures and corresponding density of states the for structures a) buckled B-AsP and b) puckered Pu-AsP. Zero of energy is set to Fermi level shown by dashed line. (For interpretation of the references to color in this figure legend, the reader is referred to the web version of this article.)

Fig.3: Relaxed geometries for the 4x4 supercells, the total and projected density of states plots for the defected structures on the B-AsP monolayer (a) V_{As} b) V_P c) V_{AsP} . In DOS plots, the total DOS of pristine B-AsP monolayer and the defected structure are illustrated together for better comparison. The following orbital projected DOS plots correspond to atoms around the defect.

Fig.4: Relaxed geometries for the 4x4 supercells, the total and projected density of states plots for the defected structures on the B-AsP monolayer (a) $As \leftrightarrow P$ b) As_P c) P_{As} . In DOS plots, the total DOS of pristine B-AsP monolayer and the defected structure are illustrated together for better comparison. The following orbital projected DOS plots correspond to atoms around the defect.

Fig.5: Relaxed geometries for the 4x4 supercells, the total and projected density of states plots for the defected structures on the Pu-AsP monolayer (a) V_{As} b) V_P c) V_{AsP} . In DOS plots, the total DOS of pristine B-AsP monolayer and the defected structure are illustrated together for better comparison. The following orbital projected DOS plots correspond to atoms around the defect.

Fig.6: Relaxed geometries for the 4x4 supercells, the total and projected density of states plots for the defected structures on the Pu-AsP monolayer (a) $As \leftrightarrow P$ b) As_P c) P_{As} . In DOS plots, the total DOS of pristine B-AsP monolayer and the defected structure are illustrated together for better comparison. The following orbital projected DOS plots correspond to atoms around the defect.

TABLE I: Calculated parameters for the three structures corresponding to Pu-AsP, B-AsP and P-AsP respectively. a , the lattice constant; $d(As - P)$, As-P distance;

Structure	a (Å)	b (Å)	$d(As - P)$ (Å)	E_{coh} (eV)	E_{gap} (eV)
$Pu - AsP$	3.50	4.68	2.382	4.782	0.924
$B - AsP$	3.46	-	2.393	4.802	1.858

TABLE II: Calculated results for optimized defective structures of B-AsP monolayer; E_{coh} , cohesive energy; E_{form} , formation energy, a , corrected lattice constant; μ , magnetic moment per supercell in units of Bohr magneton (μ_B) (NM is for nonmagnetic systems).

	V_{As}	V_P	V_{AsP}	$As \leftrightarrow P$	AsP	P_{As}
E_{coh} (eV)	4.729	4.734	4.719	4.806	4.783	4.826
E_{form} (eV)	2.576	1.708	2.369	0.140	-0.092	-0.084
a (Å)	13.70	13.71	13.58	13.84	13.84	13.78
$\mu(\mu_B)$	0.04	NM	NM	NM	NM	NM

TABLE III: Calculated results for optimized defective structures of Pu-AsP monolayer; E_{coh} , cohesive energy; E_{form} , formation energy, a and b , corrected lattice constants; μ , magnetic moment per supercell in units of Bohr magneton (μ_B) (NM is for nonmagnetic systems).

	V_{As}	V_P	V_{AsP}	$As \leftrightarrow P$	AsP	P_{As}
E_{coh} (eV)	4.759	4.754	4.765	4.784	4.772	4.795
E_{form} (eV)	1.739	1.336	0.926	-0.115	-0.052	1.336
a (Å)	13.95	13.97	13.94	14.00	14.02	14.00
b (Å)	18.65	18.68	18.64	18.72	18.74	18.72
$\mu(\mu_B)$	NM	1.19	NM	NM	NM	NM

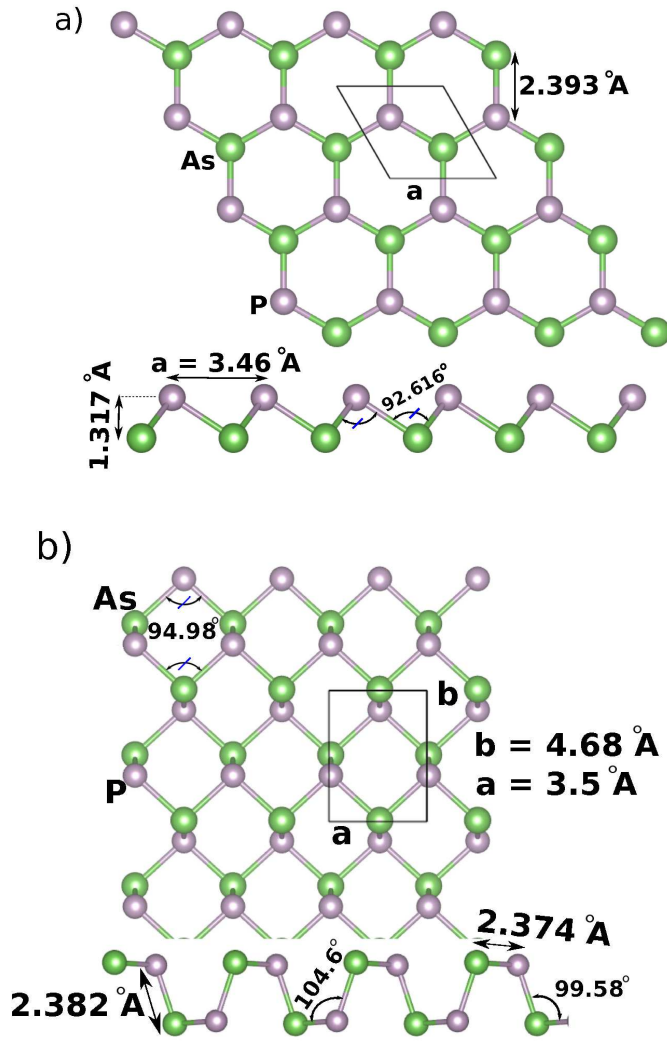


FIG. 1: Side view and top view of the structures of a) buckled B-AsP and b) puckered Pu-AsP

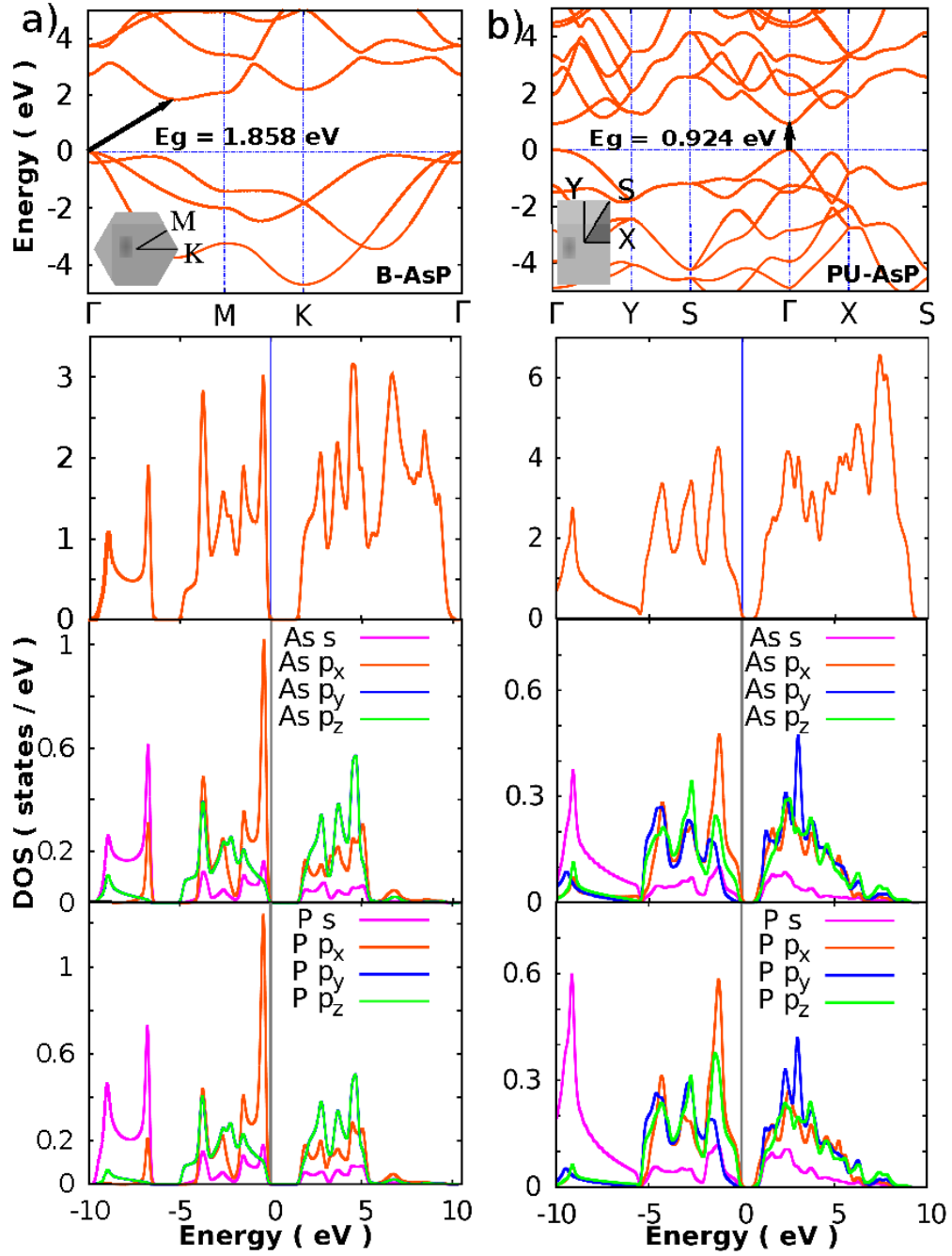


FIG. 2: Electronic band structures, corresponding total (DOS) and partial (PDOS) density of states for the monolayer structures of 1x1 a) buckled B-AsP and b) puckered PU-AsP. Zero of energy is set to Fermi level shown by dashed line. (For interpretation of the references to color in this figure legend, the reader is referred to the web version of this article.)

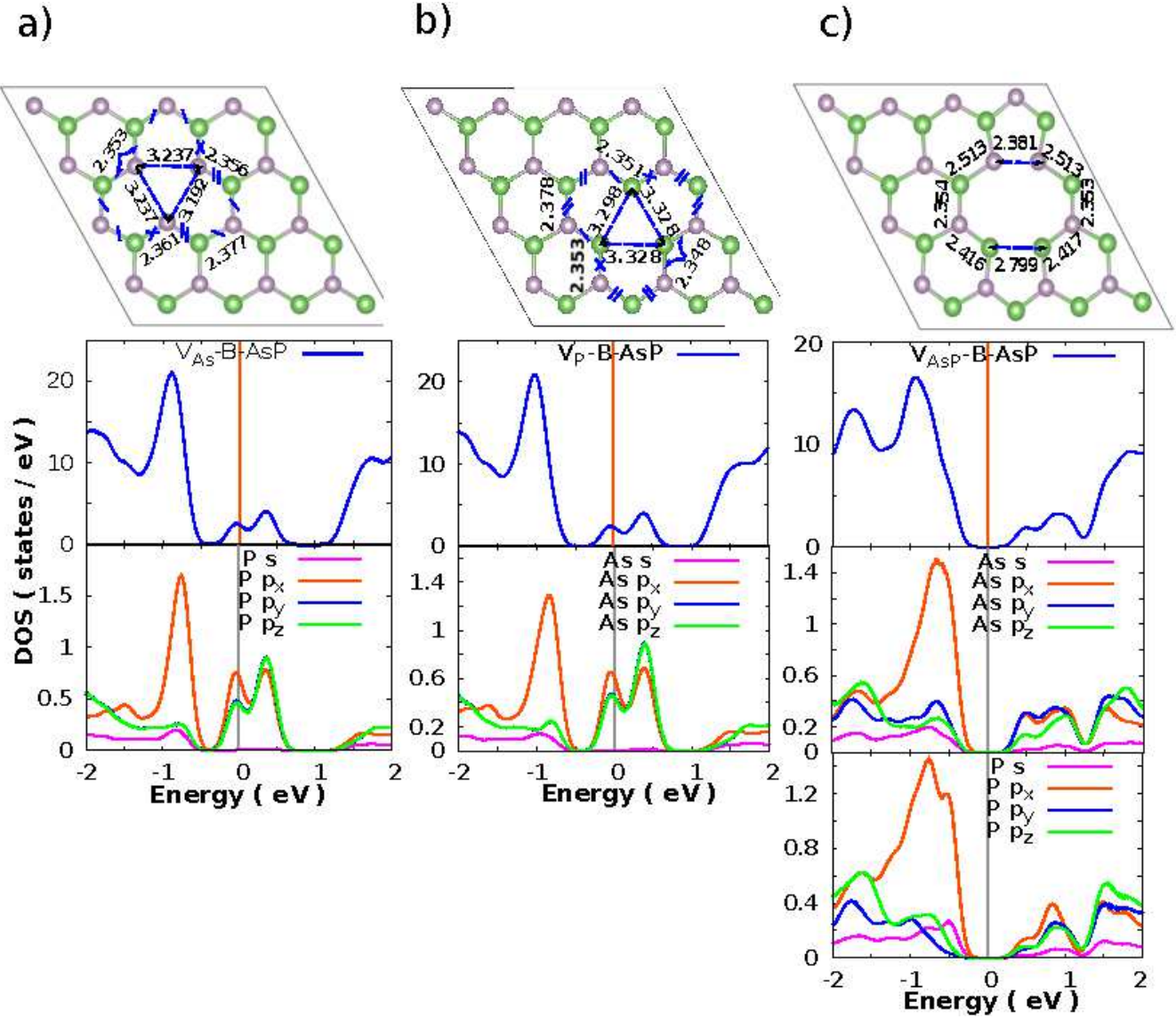


FIG. 3: Relaxed geometries for the 4x4 supercells, the total and projected density of states plots for the defected structures on the B-AsP monolayer (a) V_{As} b) V_P c) V_{AsP} . In DOS plots, the total DOS of pristine B-AsP monolayer and the defected structure are illustrated together for better comparison. The following orbital projected DOS plots correspond to atoms around the defect. All charge density plots are generated by the VESTA [47] program.

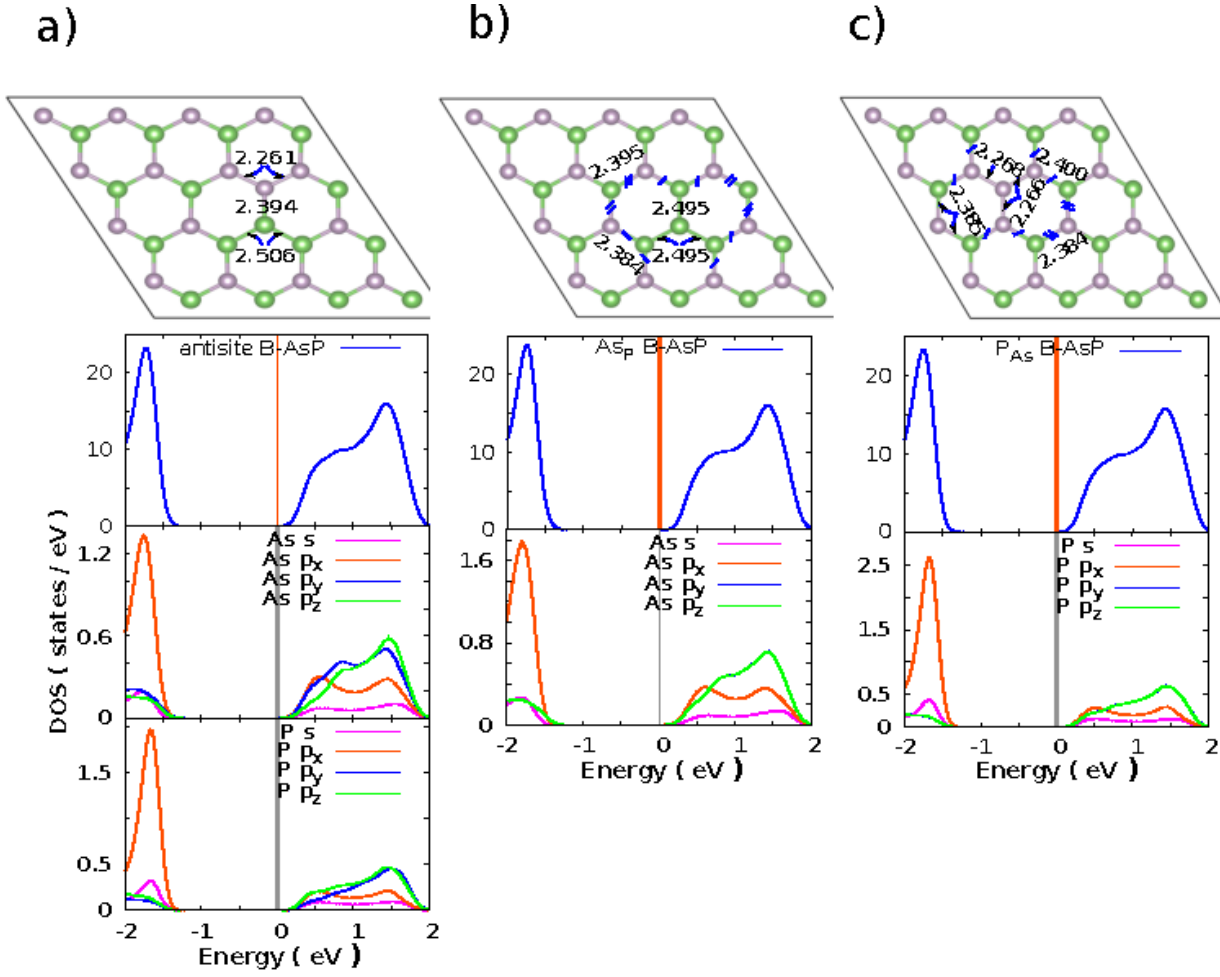


FIG. 4: Relaxed geometries for the 4x4 supercells, the total and projected density of states plots for the defected structures on the B-AsP monolayer (a) $As \leftrightarrow P$ b) As_P c) P_{As} . In DOS plots, the total DOS of pristine B-AsP monolayer and the defected structure are illustrated together for better comparison. The following orbital projected DOS plots correspond to atoms around the defect.

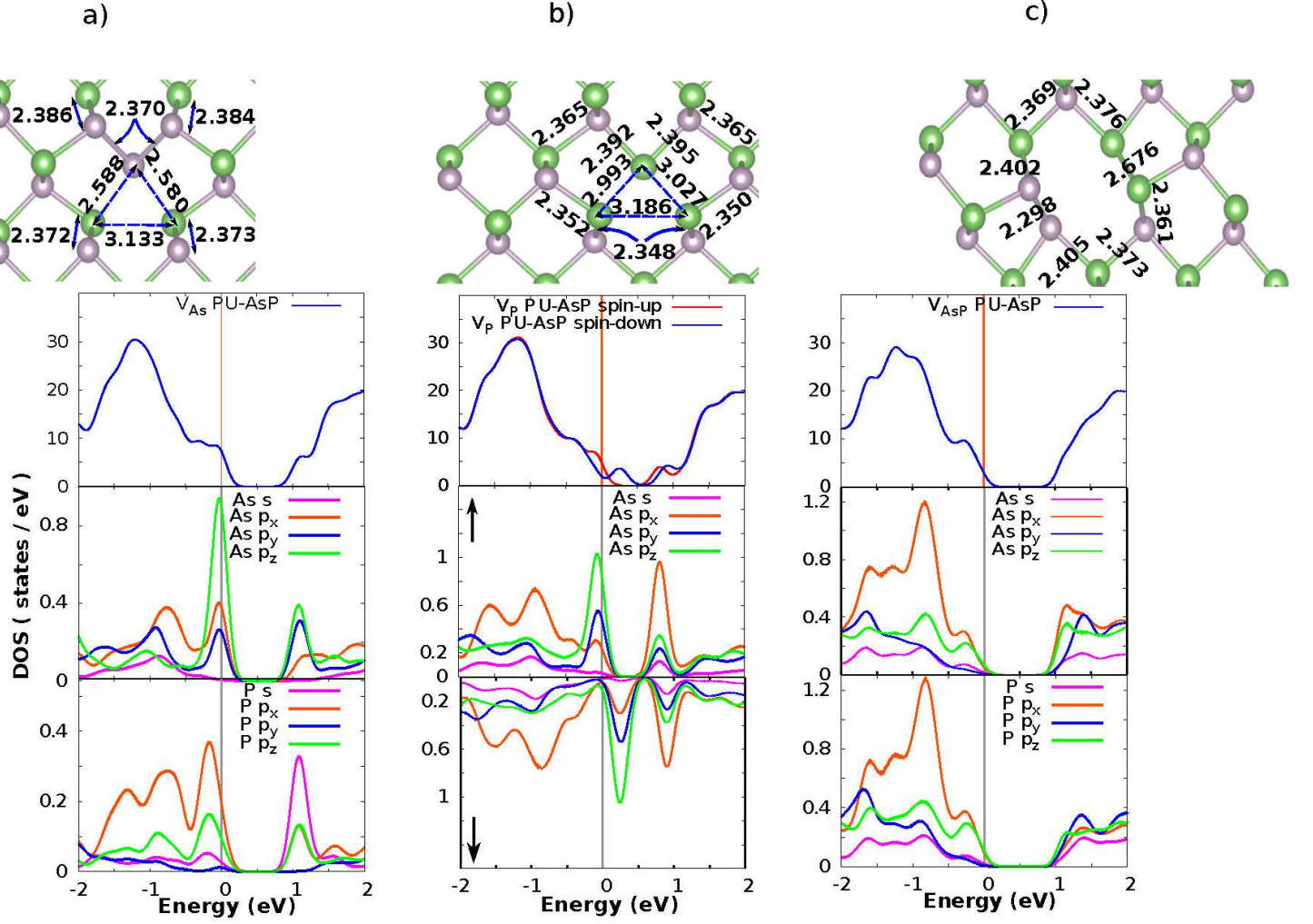


FIG. 5: Relaxed geometries for the 4x4 supercells, the total and projected density of states plots for the defected structures on the Pu-AsP monolayer (a) V_{As} b) V_P c) V_{AsP} . In DOS plots, the total DOS of pristine B-AsP monolayer and the defected structure are illustrated together for better comparison. The following orbital projected DOS plots correspond to atoms around the defect.

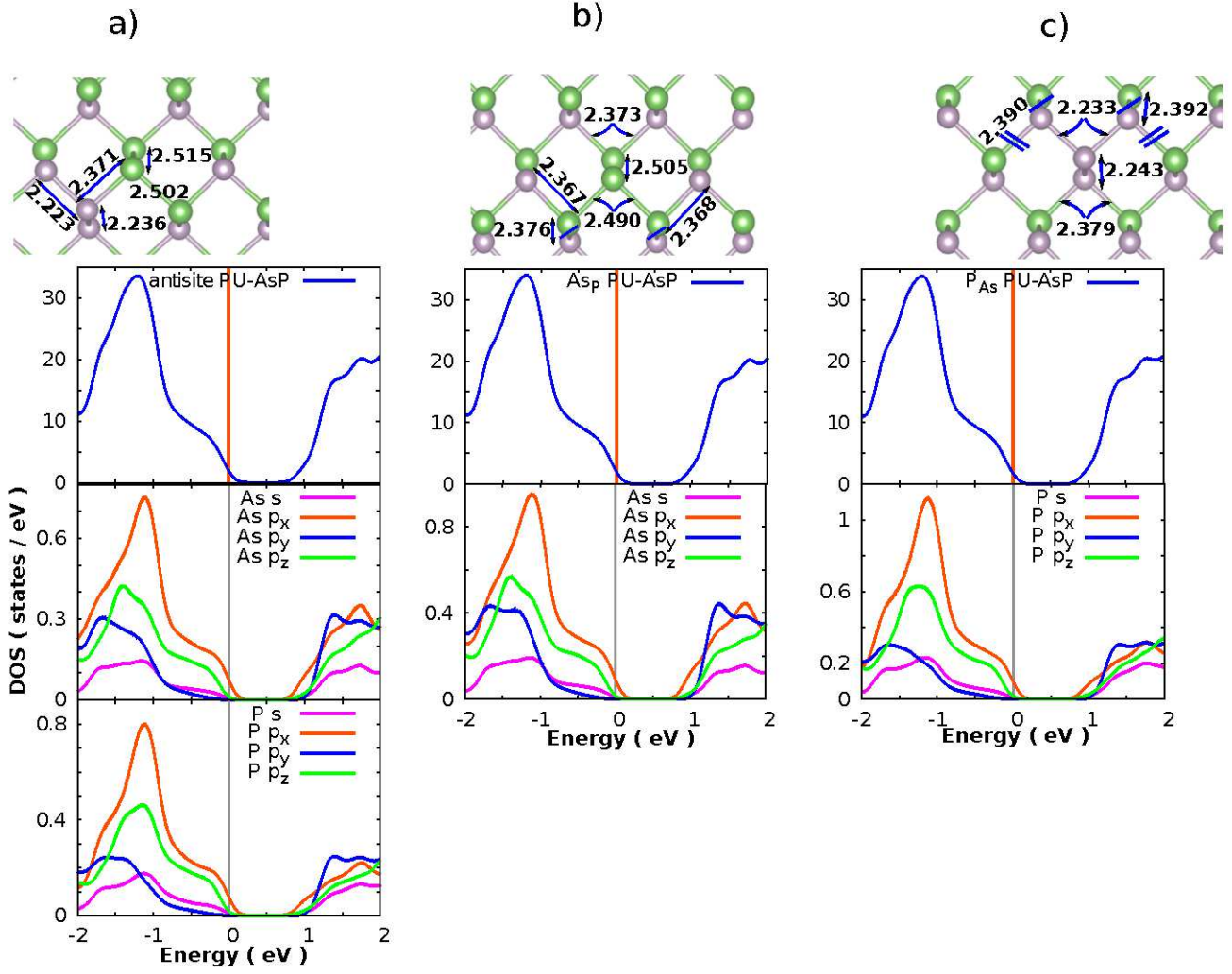


FIG. 6: Relaxed geometries for the 4x4 supercells, the total and projected density of states plots for the defected structures on the Pu-AsP monolayer (a) $As \leftrightarrow P$ (b) As_P (c) P_{As} . In DOS plots, the total DOS of pristine B-AsP monolayer and the defected structure are illustrated together for better comparison. The following orbital projected DOS plots correspond to atoms around the defect.